COBEM 2023 27TH INTERNATIONAL CONGRESS OF MECHANICAL ENGENEERING

ABCM Brazilian Society of Mechanical Sciences and Engineering
27th ABCM International Congress of Mechanical Engineering
December 04-08, 2023, Florianópolis-SC, Brazil

COB-2023-0590

Statistical features and transition dynamics of coherent organizational states in turbulent pipe flow at moderate Reynolds numbers

R. Jäckel
Mechanical Engineering Program (PEM/COPPE/UFRJ), Federal University of Rio de Janeiro, Rio de Janeiro, PC 21945-970, Brazil
Interdisciplinary Center for Fluid Dynamics, Federal University of Rio de Janeiro, Rio de Janeiro, PC 21941-594, Brazil
r.jackel@mecanica.coppe.ufrj.br
B. Magacho
B. E. Owolabi
L. Moriconi
Instituto de Física, Federal University of Rio de Janeiro, Rio de Janeiro, PC 21941-972, Brazil
Interdisciplinary Center for Fluid Dynamics, Federal University of Rio de Janeiro, Rio de Janeiro, PC 21941-594, Brazil
J. B. R. Loureiro
Mechanical Engineering Program (PEM/COPPE/UFRJ), Federal University of Rio de Janeiro, Rio de Janeiro, PC 21945-970, Brazil
Interdisciplinary Center for Fluid Dynamics, Federal University of Rio de Janeiro, Rio de Janeiro, PC 21941-594, Brazil

Abstract. *Recent advances in flow visualization techniques have provided a fascinating insight into the complex dynamics of evolving coherent structures. In turbulent pipe flow, coherent organizational states (COS), labeled by discrete azimuthal wavenumber modes, are suspected to form the state space skeleton of the turbulent dynamics, around which the chaotic dynamics are organized. In this work, through stereoscopic particle image velocimetry and conditional averaging techniques, we detect and visualize these COS in moderate Reynolds number pipe flow ($5300 < Re_D < 29000$) and study their statistical features and transition dynamics. We present, inter alia, their statistical weight contributions, streamwise organization, and transition matrices. Interestingly, the weight distribution and transition dynamics of wave number states were found to be relatively similar across all Reynolds numbers, indicating that the traditional Reynolds number effect—where turbulent statistics depend on the Reynolds number in conditions of moderate turbulence—dos not seem to be reflected in the dynamics of these COS. It turns out that the way the modes appear on the stochastic process seems to be dependent on the previous state, revealing a time correlation among the wave number modes since the Chapman-Kolmogorov equation, a necessary condition for a Markovian process, is not satisfied. The experimental results and statistical analysis offer unique insights into unexplored turbulent dynamics in pipe flow. These insights, relating to both phenomenology and statistical features, are highly relevant for improving our understanding, prediction, and modeling of turbulence.*

Keywords: *coherent states, turbulent pipe flow, dynamical systems.*

1. INTRODUCTION

Coherent states in turbulent flow are thought to present building blocks of motion with inherent patterns of morphological consistency governing the turbulent dynamics. The desire to better understand the nature of these structures has inspired continuous scientific discourse over the last two decades. Scientific discussion on turbulent structures in pipe flows is registered back to the pioneering experiments by Reynolds (1883). Since then, the focus within turbulence research has traditionally evolved around the statistical analysis of discrete flow characteristics, such as the statistical distribution of flow variables (DenToonder and Nieuwstadt, 1997), turbulent energy spectra (Meyers and Meneveau, 2008), and RANS modeling (Wu *et al.*, 2018). However, over the last few decades a new perspective has emerged to refine the description of turbulence – the dynamical systems viewpoint. It insinuates that coherent flow states correspond to local basins in the systems state space, that attract the system state on nearby trajectories, causing them to stay within and frequently return to these preferred regions (Duguet *et al.*, 2008). This understanding was sparked by considerable advancements on both experimental and numerical fronts and primarily concerns the identification and characterization of coherent structures (Grinstein and DeVore, 1996) (Chrisohoides and Sotiropoulos, 2003) (Khan *et al.*, 2020). From an experimental standpoint, the advent of technological breakthroughs such as high-resolution cameras, pulsed lasers, and advanced computer chips have ushered in the development of innovative flow visualization techniques. A prime example is time resolved Particle Image Velocimetry (PIV) which has proven suitable for capturing coherent structures through observation of complex flow field dynamics. These advanced visualization techniques have enabled the reconstruction of 2D-3C (SPIV) and 3D-3C (Tomo-PIV) flow fields, serving as the foundation for a plethora of groundbreaking studies. These publications have enriched the understanding of fluid mechanics at its core, offering intriguing glimpses into the in-

tricate dynamics of evolving coherent structures, including but not limited to traveling waves (Avila *et al.*, 2011), turbulent puffs (van Doorne and Westerweel, 2009), quasi-streamwise (Kaftori, 1993), and hairpin vortices (Dennis, 2015).

For COS in pipe flow, Hof *et al.* (2004) pioneered the effective visualization of traveling waves as coherent structures in pipe flow at Reynolds numbers bordering the laminar-turbulent transition, accomplished through SPIV experiments. The resultant structures exhibited high-speed streaks in close proximity to the wall, juxtaposed with low-speed streaks nearer to the pipe center.

Subsequently, Schneider *et al.* (2007) extended this exploration via numerical simulations, devising a novel approach for identifying structures. This new methodology unveiled a substantial variety of COS, alongside their statistical characteristics. Moreover, they hypothesized the transition dynamics could be represented as a Markovian stochastic process, a viewpoint that has been explored further in recent literature by Jäckel *et al.* (2023c).

Despite differing methods, both Hof *et al.* (2004) and Schneider *et al.* (2007) perceived traveling waves as phenomena intrinsic to the laminar-turbulent transition. This supposition, however, was challenged by the SPIV experiments of Dennis and Sogaro (2014) conducted in pipe flow at a notably turbulent regime of Re = 35000. Their results revealed that their flow too was organized into various COS, strikingly similar to traveling wave solutions observed previously only at lower Reynolds numbers.

In a very recent study, Jäckel *et al.* (2023b) were able to observe COS also in moderate Reynolds number turbulence by conditionally averaging the flow fields relative to their dominant azimuthal wave number of streamwise velocity streaks.

Notwithstanding these breakthroughs, we are merely on the precipice of fully comprehending the complex dynamics of coherent states in pipe flows. Addressing this gap is pivotal to enhancing the validation, refinement, and potential reformulation of current scientific discourse. Moreover, it is widely accepted that turbulent statistics for the logarithmic region below Reynolds numbers of 25000 lack universality, owing to their Reynolds number dependence – an occurrence frequently referred to as the Reynolds number effect (DenToonder and Nieuwstadt, 1997) (Zhou *et al.*, 2021). The question of whether this unique behavior extends to coherent structures remains a topic of ongoing debate. In this article, by means of a sophisticated flow imaging system, together with the application of dimensionality reduction techniques, we aim to take a significant stride towards the unraveling of these phenomena, venturing further into the exploration and understanding of coherent states in pipe flows.

2. METHODOLOGY

2.1 Experimental setup and conditions

The experiment was performed in a flow loop with an incorporated SPIV for flow visualization system tailored for the research on wall turbulence and coherent structures in the facilities of the Interdisciplinary Center of Fluid Dynamics (NIDF). Although detailed description and performance validation of this setup have been provided by Jäckel *et al.* (2013a), a brief overview will be given in the following. The flow loop consists of a horizontal 6-inch diameter pipe operating in a closed system as shown in Fig. 1.

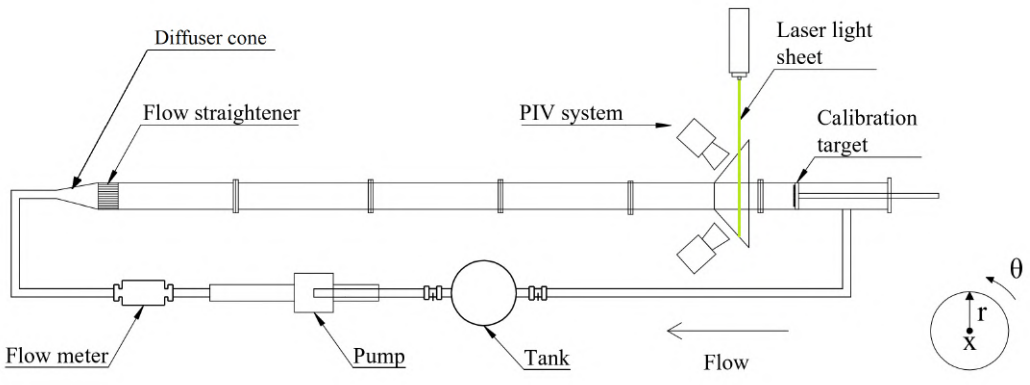

Figure 1: Experimental setup (not to scale) and coordinate system of the pipe rig with SPIV system. The flow direction is clockwise.

The rig includes a settling chamber with a diffuser cone followed by a honeycomb and a pair of screens, all aimed at reducing eddies and swirls before the flow enters the pipe. All relevant operation conditions (flow rate, water temperature, static pressure, and pump motor frequency) are monitored throughout each experiment run. The flow is seeded with quasi-neutrally-buoyant silver-coated hollow glass spheres ($\rho_p = 0.9kg\ m^{-3}$) with an average size of 17 microns. Under the assumption of Stokes flow around the particle ($Re_p < 1$), the particle Stokes number was estimated to be ap-

proximately 10^{-4} for the highest Reynolds number investigated in this study, indicating a suitable tracing behavior of the particles. Flow visualization is achieved using a time-resolved SPIV setup equipped with two high-speed CMOS cameras (Phantom Speed-sense M310). The cameras are oriented horizontally, at a 45-degree angle to the pipe centerline, pointing downstream to capture a transverse plane of the flow. The transverse laser beam is generated by a pulse-controlled flashlamp-pumped Nd:YAG laser (Litron Nano L 200-15 PIV), providing a 532 nm beam wavelength with a max. pulse energy of 200 mJ. The PIV calibration, timing, acquisition, and image processing are managed using a commercially available software package (Dantec DynamicStudio v.2015a). The software's inbuilt PIV routine employs pixel cross-correlation to determine the average particle displacement within individual interrogation areas (IAs) across sequential image frames. These frames are captured with regulated inter-frame times, allowing for the reconstruction of instantaneous 2D-3C vector fields. All Reynolds number measurements were recorded in double frame mode at a sampling frequency of 15 Hz, yielding approximately 2×10^4 captured vector fields for each experimental run. Tab. 1 shows the experimental schedule together with the most relevant parameters, where the exact Reynolds was derived from the flow rate and the temperature dependent fluid properties.

Table 1: Experimental schedule and measurement parameters.

Exact Re	**# Acquisitions**	**Measured length [R]**	**Taylor length scale [R]**
5320	22110	308	$28\ x10^{-3}$
12017	20100	628	$62\ x10^{-3}$
17816	18090	829	$92\ x10^{-3}$
24414	20100	1259	$125\ x10^{-3}$
29089	20100	1492	$148\ x10^{-3}$

2.2 Detection of coherent organizational states

To detect and visualize coherent structures within a state space, one can utilize dimensionality reduction techniques which aim to encapsulate the essential characteristics of the system's dynamics. In this work, the detection of coherent states is based on observing the occurrences of the alternating pattern of positive and negative fluctuations in streamwise velocity component u along the azimuthal dimension within each vector field snapshot, as described in detail by Jäckel *et al.* (2023b). The elongated, meandering regions of high and low momentum fluid along the pipe, also known as streaks, are advected in the direction of the mean flow.

For the detection, a reference point (r_0, θ_0) is defined together with the spatial correlation function R_{uu} between the reference point and equally distributed points located along the $r = r_0$ circumference with an azimuthal spacing of $\Delta\theta$ by means of Eq. 1:

$$R_{uu}(r_0 + \Delta r, \Delta\theta) = \frac{\langle u(r_0 + \Delta r, \theta_0 + \Delta\theta)\ u(r_0, \theta_0)\rangle}{u_{rms}^2} \tag{1}$$

where the azimuthal spacing of $\Delta\theta$ has a resolution of 72 equally spaced azimuthal points. Note that the square brackets indicate an azimuthal average over the initial angles θ_0. By limiting Eq. 1 to a fixed radius of interest, here $r_0 = 0.78R$, it turns into an azimuthal correlation function which will be used for the state detection. This is done through the determination of the azimuthal wave number of each snapshot by taking the highest value of the power of the Fast Fourier Transform (FFT) on the azimuthal correlation, which relates the flow field to a well-defined wave number-labeled state. In this way, the complex pattern of a 3-dimensional flow field is reduced to a single parameter, i.e. the azimuthal wave number, to which each snapshot gets assigned. Fig. 2 (top row) showcases examples of instantaneous snapshots of velocity field fluctuations at Re = 17800, with red and blue representing velocities above and below the 1.5 % mean velocity profile envelope. These snapshots, assigned to azimuthal wave numbers 2, 3, and 4 using our detection method, demonstrate that even though small-scale fluctuations dominate the background, the dominant streak patterns along the azimuth distinctly reflect their respective wave numbers. We can also extend the azimuthal correlation over a radial grid spaced at 1 mm intervals to visualize the spatial correlation R_{uu} across the entire cross-stream plane as shown in Fig. 2 (bottom row) for the wave numbers 2, 3, and 4. Note that R_{uu} is represented by iso-contours in relation to the reference point, the location of which is marked by a black dot. The red level curves correspond to R_{uu} values of 0.05 and 0.1, while the blue curves represent values of the opposite sign.

In order to visualize the spatial distribution of the COS along the stream direction, we can apply Taylor's hypothesis (Taylor, 1938) (Dennis and Nickels, 2008). This has been done for the ten dominant wave number states, as shown in Fig. 3.

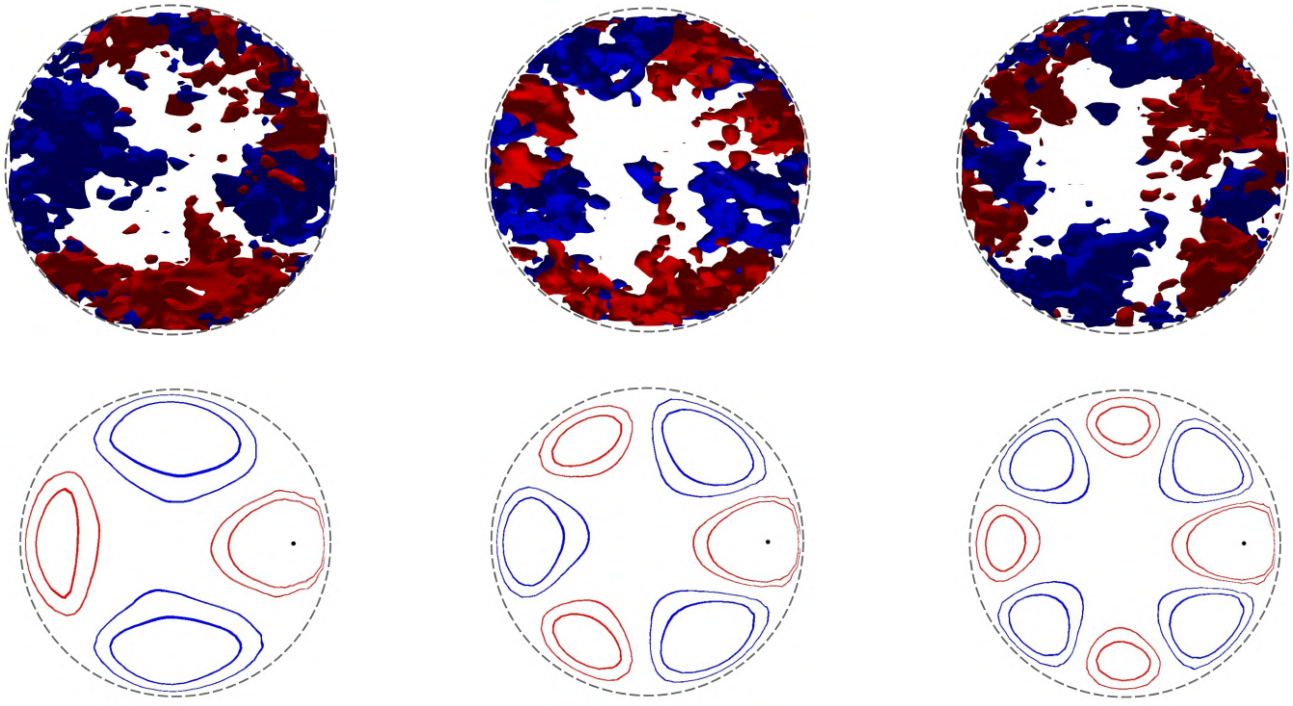

(a) $k_\theta = 2$ (b) $k_\theta = 3$ (c) $k_\theta = 4$

Figure 2: Coherent states with azimuthal wave numbers 2, 3, and 4 for Re = 17800. The top row includes snapshots of associated velocity field fluctuations. The bottom row depicts the corresponding spatial correlation function, where red curves indicate R_{uu} = 0.05 and 0.1, and blue curves denote the inverse.

At first glance, several wave number structures with a streamwise extent approximately on the order of the pipe radius can be identified, particularly in the range of wave numbers 1 to 6. These structures are longer and less intermittent. However, for the remaining wave number states, the structures appear more sporadic and include several instances of single-snapshot observations. These observations hint that the wave number states do indeed exhibit a streamwise correlation, with a marked tendency to appear in clusters of consecutive occurrences.

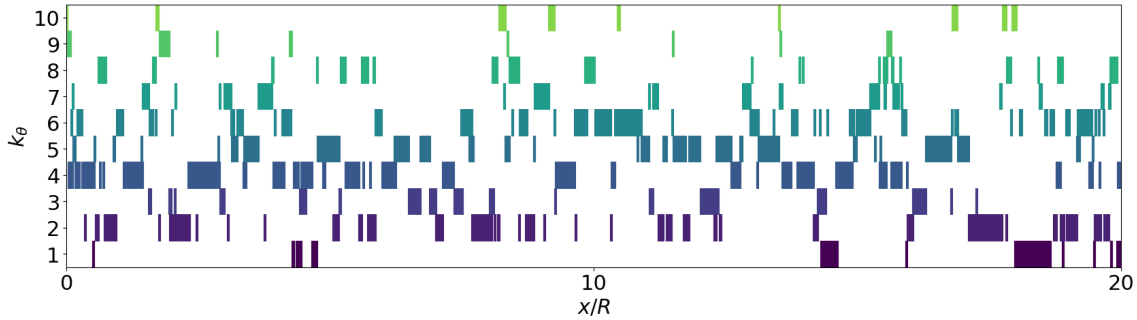

Figure 3: Streamwise extent of coherent states along the main flow direction in an arbitrary section 20 pipe radii at Re = 17800.

To explore this observation in a more quantitative way, we can construct a transition probability matrix based on the wave number snapshot observations. This will allow us to quantify the dynamics of the wave number transitions and their propensity to persist.

Therefore, we define T_{ij} as the transition probability matrix for a specific Reynolds number. Each element, ij, represents the probability that a given state, i, will transition to a state, j, hence:

$$T_{ij} = \sum(k_{\theta_i} \to k_{\theta_j}) / \sum k_{\theta_i} \tag{2}$$

Note that the sum of the elements in each column equals one, assuming azimuthal wave number states k_θ ranging from 1 to 10.

Fig. 4 exemplarily shows the wave number snapshot transition probabilities for Re = 17800, using a contour heat map to present the underlying transition probability matrix. We observe that the probabilities along the diagonal are elevated, which reveals a tendency for the wave number to persist over several consecutive instances. This can be depicted as a clearly dominant feature of the system's behavior and was observed for all Reynolds numbers.

In this context, as a logical consequence we shift our perspective from the viewpoint of individual snapshots to that of structures. Here, a structure is defined as a consecutive series of snapshot observations with the same wave number. Single wave number observations, which often appear in sequences of alternating wave number snapshots, are defined as unstable remainders that constitute to chaotic trajectories in the phase space. These can be interpreted as paths that connect the attractors (or basins) of coherent states, which are preferentially visited by the system.

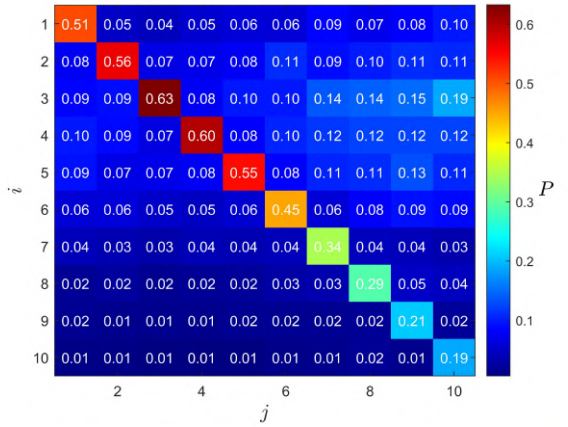

Figure 4: Wave number snapshot transitions probabilities indicating the transition probability (P) from a snapshot of wave number state i to wave number state j for the Re = 17800.

2.3 Convergence of Statistics

Before deepening the analysis of the system's statistical features, it is crucial to ascertain whether its statistics demonstrate convergence with an increasing number of wave number samples. Therefore, the statistical contributions of wave numbers were evaluated from both the snapshot and the structure perspectives. It was found that for all Reynolds numbers, the wave number statistics exhibited asymptotic behavior starting from $\sim 10^4$ samples or even earlier. Fig. 5 a) and b) exemplify the convergence behavior of Re = 17800 (the experiment with least available sample contributions as shown in Tab. 1) for the wave number distribution statistics from the snapshot's and structure's perspectives, respectively. It is evident that the sub-sample interval curves align with the line representing all data points when the sample size reaches approximately 10^4. This convergence of the statistics with an increasing number of samples ensures that the subsequent analysis of the system's behavior will be based on a reliable representation of the full range of wave number dynamics, which in turn allows for accurate insights into the system's structure.

3. RESULTS AND DISCUSSION

We begin by presenting the statistical weight distributions, specifically the percentage contributions of the ten most dominant states relative to the total count of wave number-assigned vector fields, as depicted in Fig. 6 a). No threshold has been applied in this case.

The weight distributions exhibit positive skewness towards lower states for all Reynolds numbers studied. For all cases, the state detected most frequently was wave number 3. This finding aligns with previous observations Dennis and Sogaro (2014) for Re = 35000 and the most energetic azimuthal mode identified via POD in turbulent pipe flow at Re = 24580 in the DNS study by Baltzer *et al.* (2013).

Among the ten dominant wave numbers, state 10 displayed the lowest statistical weight. Although wave number states exceeding 10 were also detected, their statistical contribution was minimal (less than 1 per cent in all sets) and may not exhibit converged statistics. Interestingly, the highest wave numbers identified in each set tended to increase with rising Reynolds numbers.

Fig. 6 b) illustrates the normalized distribution of wave number structures that possess a streamwise extent. This representation is unique because the statistical weight distribution is calculated in relation to the number of distinct structures traversing the measurement plane, rather than being solely based on the raw count of snapshots associated with wave number sets. Since our analysis focused on structures with a streamwise extent, vector fields that were only captured in a single snapshot, which were previously categorized as unstable remainder contributions, have been excluded from this

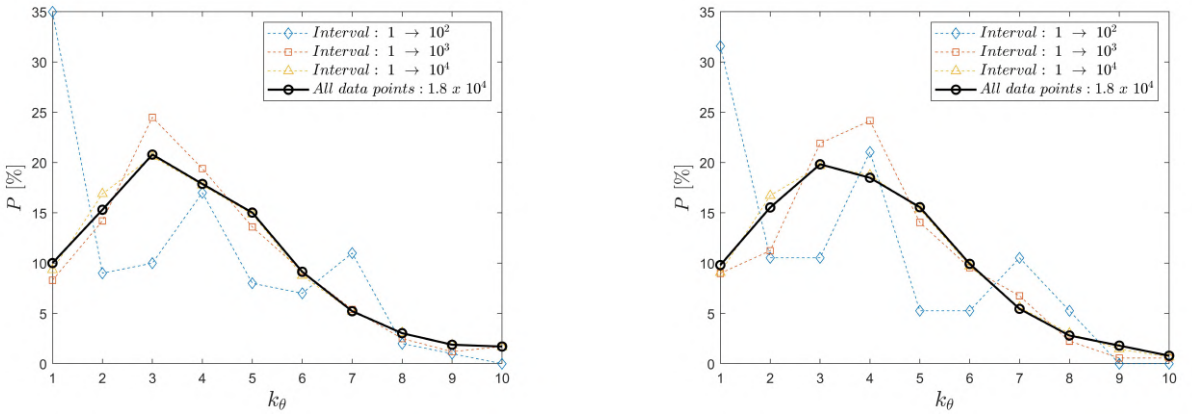

(a) Convergence snapshots

(b) Convergence structures

Figure 5: Analysis of convergence for statistical weight contributions of wave numbers for snapshots (a) and structures (b) for Re = 17800.

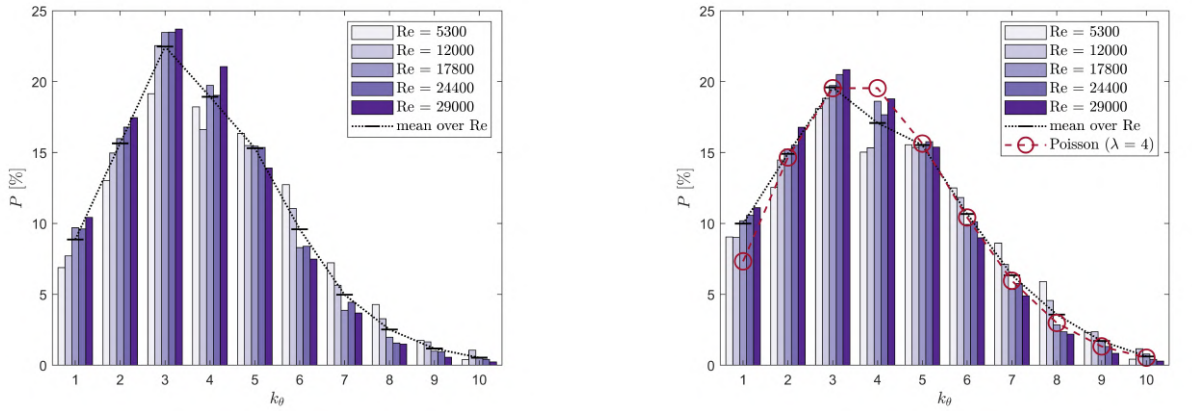

(a) snapshot distribution

(b) structure distribution

Figure 6: Normalized distribution of dominant wave number states based on snapshot (a) and structure (b) observations.

representation. Despite their exclusion, it is important to note that these remainders have a significant contribution to the overall weight. The range from one-fourth to one-third of all observations, with their presence increasing alongside the Reynolds number, an indication that generally the recurrence time-scale of the structures is increasing.

Comparing Figs. 6 a) and b), it becomes apparent that from the structure's perspective, higher wave number structures contribute less weight than from the snapshot's viewpoint. We interpret this as an indication of the more intermittent behavior of higher wave number states, often manifesting as unstable remainder states in the structure representation.

Both from the snapshot's and the structure's perspective, the weight distribution of states appears generally unaffected by the Reynolds number. Upon closer inspection, a very slight shift to the right with increasing Reynolds number is observable, indicating that higher wave number states become marginally more frequent with increasing Reynolds numbers.

An intriguing statistical observation from Fig. 6 b) is that the mode distributions closely resemble a Poisson distribution $P(k_\theta, \lambda = 4)$. In general, a Poisson distribution with an arbitrary parameter λ can be expressed as:

$$P(k_\theta, \lambda) = \frac{\lambda^{k_\theta} e^{-\lambda}}{k_\theta!} \, . \tag{3}$$

The Poisson-like distribution may suggest that the transitions between modes follow a Markovian process. In essence, a Markovian process is one in which the future state depends solely on the present state, and not on any past states. This satisfies the Chapman-Kolmogorov (CK) equation. To illustrate this, let's consider K_1 and K_2 as two random variables defined at two time instants $t_1 > 0$ and $t_2 > t_1$ with probabilities $P(K_1)$ and $P(K_2)$, respectively. The CK equation can be written as:

$$P(K_2) = \int dK_1 P(K_2|K_1) P(K_1) \, , \tag{4}$$

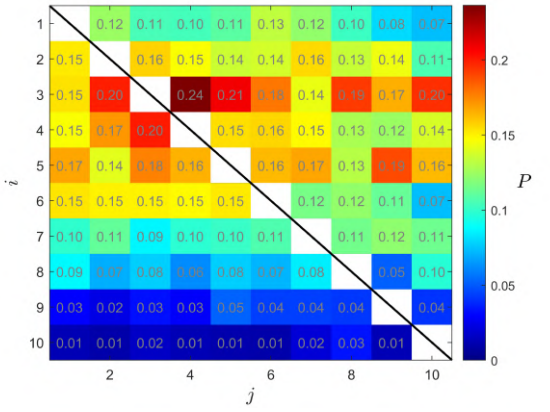

(a) Re = 5300

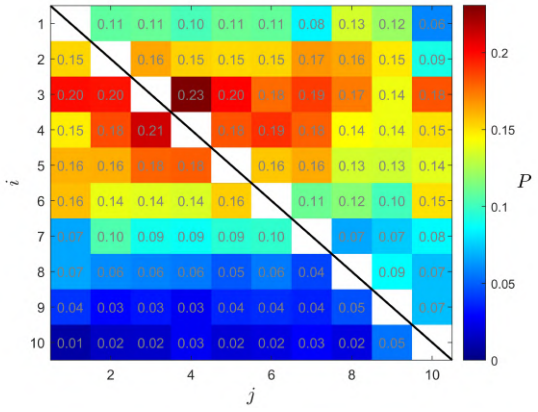

(b) Re = 12000

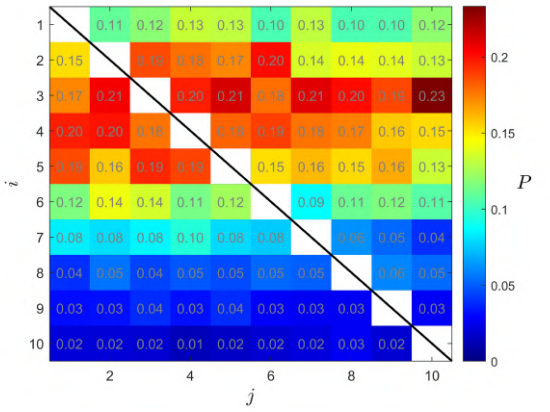

(c) Re = 17800

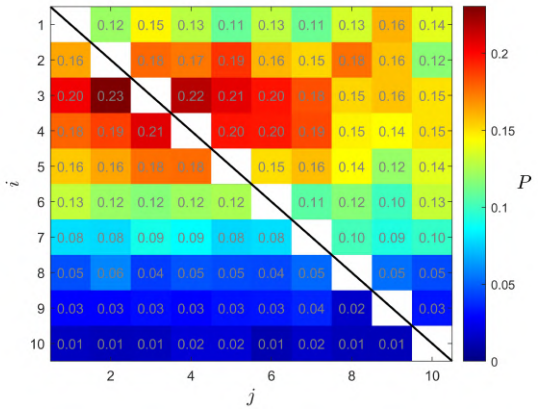

(d) Re = 24400

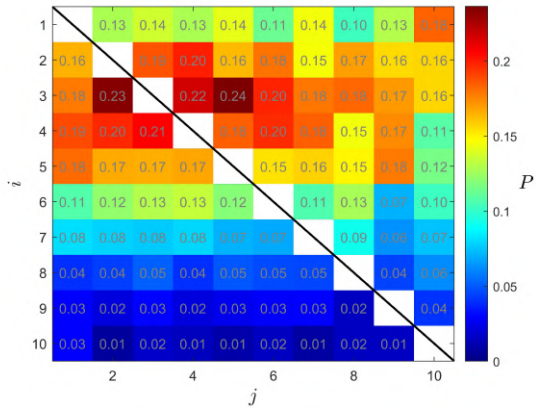

(e) Re = 29000

Figure 7: Wave number structure transitions probabilities indicating the transition probability (P) from a structure of wave number state i to wave number state j for the Re = 5300, 12000, 17800, 24400, and 29000.

where $P(K_2|K_1)$ is the conditional probability of observing K_2 given that K_1 was observed. If we pick K_2 independently of K_1, for example by the Poisson distribution from Eq. 3, the CK equation is immediately satisfied, suggesting a Markovian process (a necessary but not sufficient condition).

However, the reality of how modes appear in this stochastic process appears to deviate from this assumption. It seems that the appearance of a mode is dependent on the previous state, indicating a time correlation among the modes (see Jäckel *et al.* (2023c)). This deviates from the expectations of a pure Markovian process and suggests a more intricate underlying dynamic, as is has been suggested in earlier studies (Schneider *et al.*, 2007).

Fig. 7 displays the transition probabilities of number structures, indicating the probability of transitioning from wave number state i to wave number state j for all studied Reynolds numbers. The matrix diagonal has been deliberately omitted since the probability to persist does not apply for the structure's perspective. As one might infer from the wave number distributions in Fig. 6, transitions predominantly occur within wave number states 2 to 6, with the highest probabilities along state 3, across all Reynolds numbers.

It is interesting that both the transition dynamics and state distributions remain relatively consistent across the range of studied Reynolds numbers. This suggests that the earlier-mentioned Reynolds number effect, i.e., the dependence of turbulent statistics on Reynolds numbers in the range of moderate Reynolds numbers, is not mirrored from the perspective of coherent states in dynamical systems.

4. CONCLUSIONS

In this study, we explored the statistical features and transition dynamics of coherent organizational states within turbulent pipe flow at moderate Reynolds numbers. The data was obtained through flow field imaging using a SPIV system. To decipher the essential characteristics of the system's dynamics, a dimensionality reduction technique based on detecting the count of velocity streaks along the pipe's azimuth was applied. Our key observations are presented in the following:

1. Across all examined Reynolds numbers, ten dominant states comprising alternating streak patterns along the pipe's azimuth were consistently identified, confirming that coherent states are a pervasive feature of fully developed turbulent pipe flow, not merely phenomena of laminar-turbulent transition. The weight distribution of these states, skewed positively towards lower states with a most frequently encountered azimuthal wave number of 3, is well described by a Poisson distribution. This suggests that transitions between wave number structures occur independently of the current state.

2. Interestingly, the weight distribution and transition dynamics of wave number states were found to be relatively similar across all Reynolds numbers, indicating that the traditional Reynolds number effect—where turbulent statistics depend on the Reynolds number in conditions of moderate turbulence—dos not seem to be reflected in the dynamics of these coherent states.

3. It turns out, that the way the modes appear on the stochastic process seems to be dependent on the previous state, revealing a time correlation among the wave number modes since the CK equation, a necessary condition for a Markovian process, is not satisfied.

5. ACKNOWLEDGEMENTS

This research received parcial financial support from the Brazilian National Council for Scientific and Technological Development (CNPq) and Petrobras (ANP/Petrobras 5850.0104954.17.9 and 0050.0122372.22.9). Further, the authors gratefully acknowledge support from Shell Brasil through the project "Predictive modelling of inorganic scaling in pipes and equipment subjected to multiphase flows in Pre-Salt conditions" at the Interdisciplinary Center of Fluid Dynamics (NIDF) and the strategic importance of the support given by ANP through the R&D levy regulation.

6. REFERENCES

Avila, K., Moxey, D., Lozar, A.D., Avila, M., Barkley, D. and Hof, B., 2011. "The onset of turbulence in pipe flow". *Science*, Vol. 333, p. 192.

Baltzer, J.R., Adrian, R.J. and Wu, X., 2013. "Structural organization of large and very large scales in turbulent pipe flow simulation". *J. Fluid Mech.*, Vol. 720, pp. 236–279.

Chrisohoides, A. and Sotiropoulos, F., 2003. "Experimental visualization of lagrangian coherent structures in aperiodic flows". *Phys. Fluids*, Vol. 15, p. L25.

Dennis, D.J.C., 2015. "Coherent structures in wall-bounded turbulence". *Annals of the Brazilian Academy of Sciences*, Vol. 87(2), p. 1161.

Dennis, D.J.C. and Nickels, T.B., 2008. "On the limitations of taylor's hypothesis in constructing long structures in a turbulent boundary layer". *J. Fluid Mech.*, Vol. 614, p. 197.

Dennis, D.J.C. and Sogaro, F.M., 2014. "Distinct organizational states of fully developed turbulent pipe flow,". *Phys. Rev. Lett.*, Vol. 113, p. 234501.

DenToonder, J.M.J. and Nieuwstadt, F.T.M., 1997. "Reynolds number effects in a turbulent pipe flow for low to moderate re". *Phys. Fluids*, Vol. 9, p. 3398.

Duguet, Y., Pringle, C.C.T. and Kerswell, R.R., 2008. "Relative periodic orbits in transitional pipe flow". *Physics of Fluids*, Vol. 20, p. 114102.

Grinstein, F.F. and DeVore, C.R., 1996. "Dynamics of coherent structures and transition to turbulence in free square jets". *Phys. Fluids*, Vol. 8, p. 1237.

Hof, B., VanDoorne, C.W.H., Nieuwstadt, F.T.M., Faisst, H., Eckhardt, B., Wedin, H., Kerwell, R.R. and Waleffe, F., 2004. "Experimental observation of nonlinear traveling waves in turbulent pipe flow". *Science*, Vol. 305, p. 2004.

Jäckel, R., Magacho, B., Owolabi, B., Moriconi, L., Dennis, D.J.C. and Loureiro, J.B.R., 2023c. "Stochastic model of organizational state transitions in a turbulent pipe flow". *Phys. Rev. Fluids*, Vol. 8, p. 064609.

Jäckel, R., Magacho, B., Owolabi, B.E., Moriconi, L., Dennis, D.J.C. and Loureiro, J.B.R., 2023b. "Coherent organizational states in turbulent pipe flow at moderate Reynolds numbers". *Physics of Fluids*, Vol. 35, p. 045127.

Jäckel, R., Owolabi, B., Magacho, B., Moriconi, L., Dennis, D. and Loureiro, J., 2013a. "A large-scale experiment for the visualization of near-wall structures in turbulent pipe flow using stereoscopic piv". In *Proceedings of the 8th International Conference on Multiphase Flow and Heat Transfer (ICMFHT 2023)*. ICMFHT, Lisbon, Portugal.

Kaftori, D., 1993. *Structures in the turbulent boundary layer and their interaction with particles*. University of California, Santa Barbara.

Khan, H.H., Anwer, S.F. and H, N., 2020. "Dynamics of coherent structures in turbulent square duct flow". *Phys. Fluids*, Vol. 32, p. 045106.

Meyers, J. and Meneveau, C., 2008. "A functional form for the energy spectrum parametrizing bottleneck and intermittency effects". *Physics of Fluids*, Vol. 20, p. 065109.

Reynolds, O., 1883. "An experimental investigation of the circumstances which determine whether the motion of water shall be direct or sinuous, and of the law of resistance in parallel channels". *Proc. Royal Soc.*, Vol. 35, p. 84.

Schneider, T.M., Eckhardt, B. and Vollmer, J., 2007. "Statistical analysis of coherent structures in transitional pipe flow". *Phys. Rev. E*, Vol. 75, p. 066313.

Taylor, G.I., 1938. "The spectrum of turbulence". *Proc. R. Soc.*, Vol. 164, p. 476.

van Doorne, C.W. and Westerweel, J., 2009. "The flow structure of a puff". *Philosophical Transactions of the Royal Society A: Mathematical, Physical and Engineering Sciences*, Vol. 367, pp. 489–507.

Wu, J.L., Xiao, H. and Paterson, E., 2018. "Physics-informed machine learning approach for augmenting turbulence models: A comprehensive framework". *Phys. Rev. Fluids*, Vol. 3, p. 074602.

Zhou, Z., Wu, T. and Yang, X., 2021. "Reynolds number effect on statistics of turbulent flows over periodic hills". *Phys. Fluids*, Vol. 33, p. 105124.

7. RESPONSIBILITY NOTICE

The authors are solely responsible for the printed material included in this paper.